J Mater Sci (2016) 51:7699–7715

The usability of recycled carbon fibres in short fibre thermoplastics: interfacial properties

D. T. Burn[1], L. T. Harper[1,*], M. Johnson[1], N. A. Warrior[1], U. Nagel[2], L. Yang[2], and J. Thomason[2]

[1] *School of Mechanical, Materials and Manufacturing Engineering, University of Nottingham, The ITRC Building, University Park, Nottingham NG7 2RD, UK*

[2] *Department of Mechanical Engineering, University of Strathclyde, 75 Montrose Street, Glasgow G1 1XJ, UK*

Received: 29 February 2016
Accepted: 9 May 2016
Published online: 19 May 2016

ABSTRACT

The objective of this study was to investigate the feasibility of combining discontinuous recycled carbon fibres with polypropylene, to produce a low-cost, high specific stiffness material for high-volume applications. The inherent low affinity of carbon fibre and polypropylene motivated a detailed study of the surface characteristics of carbon fibre and interfacial behaviour between the two materials, using the microbond test. The effects of removing the sizing from the fibres, as well as introducing a maleic anhydride-grafted polypropylene coupling agent, were extensively investigated. Polypropylene was found to degrade when prepared under atmospheric conditions; therefore, it was necessary to form droplets under nitrogen. Removal of the sizing from the fibre using pyrolysis and solvolysis techniques altered the surface morphology of the fibre and increased the interfacial shear strength (IFSS) by 4 and 33 %, respectively. A more significant improvement in the fibre–matrix adhesion was achieved by adding a maleic anhydride coupling agent at 2 wt%, which increased the IFSS by 320 %.

Introduction

Thermoplastic composites used in the automotive industry are primarily injection moulded to yield cycle times of less than 1 min, but this processing route limits fibre length to less than 1 mm and therefore restricts the achievable mechanical performance. Long fibre thermoplastics (LFTs) are able to maintain a marginally longer fibre length (2–3 mm) due to a less aggressive processing route [1], but the main limitation is that in-mould melt flow distances can be quite large, limiting fibre volume fractions to around 25 % [2].

For non-structural automotive parts, glass fibre is most commonly combined with thermoplastic matrices, with the average cost of a finished carbon fibre part costing 50 % more than with glass fibre [3]. The high manufacturing costs for carbon fibre limit applications to niche areas where mechanical properties and mass reduction are of paramount importance. Studies have shown that recycling carbon fibre can reduce the cost by almost 50 % compared to the

Address correspondence to E-mail: lee.harper@nottingham.ac.uk

DOI 10.1007/s10853-016-0053-y

virgin fibre [4]. With future prices of virgin carbon fibre unlikely to fall below £14/kg [3], the use of recycled fibres seems compelling. This creates an opportunity for developing lower-cost, carbon fibre-reinforced thermoplastics suitable for high-performance, high-volume applications.

Polypropylene is a commodity thermoplastic belonging to the polyolefin group, which is widely used due to its low cost, high toughness and excellent chemical resistance [5]. However, polymers from this group are nonpolar and therefore have a low chemical affinity with other materials. They can only interact with fibres through physical or mechanical interaction, such as compressive radial stresses formed during cooling [6]. Additionally, carbon fibre is typically coated with an epoxy compatible sizing which may not be compatible with thermoplastic matrices; therefore achieving good interfacial adhesion between carbon fibre and polypropylene is challenging. Tang and Kardos [7] note that for improvement of interfacial adhesion, the sizing must be optimised for the specific fibre and matrix combination used; here, the sizing present on the fibres was optimised for epoxy composites. A recent study by Dai et al. [8] showed that even in carbon fibre/epoxy composites with sizing optimised for epoxy, sizing removal can result in a 10 % increase in IFSS. This has been demonstrated by Maligno et al. [9] where finite element studies have shown that sizing can have an adverse effect on the interfacial behaviour, if the stiffness is lower than the fibre/matrix materials. This can be a critical problem as the mechanical performance of discontinuous fibre composites is strongly influenced by the microscale interface, which is responsible for transferring shear stress between the discontinuous fibres and the matrix. Greco et al. [10] investigated oxidative thermal and nitric acid treatments to improve the adhesion of recycled carbon fibres after the sizing had been removed. The IFSS for the pyrolysis-prepared fibres was dominated by friction between the fibre and matrix surfaces; however, this could be improved further by increasing the oxygen content at the interface through chemical treatment.

The mechanical properties of composites manufactured with polyolefin matrices can be improved, however, by introducing a coupling agent to promote the chemical interaction with the fibre [11–14].

The influence on the interface strength of adding maleic anhydride to glass fibre is well documented, with a number of authors finding that adding small percentages (typically around 2 wt%) of the coupling agent to polypropylene can significantly increase the interface strength. Yang and Thomason [15] found that adding 2 wt% of maleic anhydride gave an increase in IFSS of 46 and 111 % for the microbond and single fibre pull-out test, respectively. Jannerfeldt et al. [16] also used a 2 wt% addition and found a 27 % increase in IFSS over the unmodified polymer using the microbond test. A 5 wt% addition to polypropylene used with basalt fibres increased the IFSS by 100 %, yielding comparable values to a carbon fibre/epoxy system. The study of adhesion between carbon fibre and polypropylene has not, however, been widely covered. Wong et al. [12] investigated the effect of three types of maleic anhydride, with varying weight average molecular weights (9100–52,000) ranging between 0–8 wt% on recycled carbon fibre. The authors found that adding the coupling agent at 2 wt% increased the IFSS between 100 and 200 % for the different types of maleic anhydride. Further increases in maleic anhydride content resulted in minimal increases in IFSS, with 8 wt% giving a 225 % increase over the unmodified polymer. The maximum IFSS that the authors achieved was approximately 6.5 MPa, which was extremely low compared to GF.mPP systems (approximately, 25 MPa [15]). A suspected cause for the low interface strength results is polymer degradation, which occurs during droplet formation. It is unlikely that polymer degradation occurs during the extrusion process, but microdroplet samples are exposed to air at 210 °C, well above the melting point for PP.

The combination of low-cost thermoplastic polymers with high value carbon fibre has not been widely investigated, primarily due to the disparity in cost. However, potential cost reduction brought about by carbon fibre recycling methods and future processing developments has prompted research to understand maximum mechanical performance levels. This paper presents a study to assess the compatibility between epoxy-sized carbon fibre and polypropylene. The microdroplet method has been used to determine the influence of the fibre recycling process on the interfacial bond strength. Both pyrolysis and solvolysis processes have been used to simulate different fibre recycling approaches as used in [12], but microdroplet samples have been prepared under nitrogen-purged conditions to prevent

thermal-oxidative degradation, which is a suspected cause for the low interfacial strength results published for CF.PP to date. Additionally, a coupling agent has been added to the polypropylene to promote chemical adhesion at the fibre/matrix interface.

Experimental

Materials

Filaments were extracted from T700SC-60E 12 K carbon tows supplied by Toray Co., Ltd, since this material is widely used in commercial automotive applications. This is a high-strength (4900 MPa), standard modulus fibre (230 GPa) with 0.3 wt% epoxy sizing content (manufacturer's data quoted [17]). An isotactic homopolymer polypropylene (Sabic 576P), with a melt flow index of 19 g/10 min (at 230 °C and 2.16 kg), was used as the matrix, supplied in pellet form. A maleic anhydride-grafted polypropylene (mPP) coupling agent (Eastman G-3015) in granular form was mixed with the polypropylene at 2 wt% in a Prism TSE twin-screw extruder at 200 °C. The screw speed was 120 rpm and the feeder speed was set to 80 rpm. The extruded material was subsequently pelletised. Benchmark epoxy microbond samples were produced using a development epoxy powder system (DLS1776) [18] supplied by Hexcel, UK. The mechanical properties for these materials are presented in Table 1.

Sample preparation

Fibre sizing removal

Three fibre permutations were used for the study; T700SC virgin carbon fibre (VCF), a pseudo-recycled fibre where the sizing was removed by pyrolysis (CFP) and a pseudo-recycled fibre where the sizing was removed by solvolysis (CFS), was in accordance with [19] and manufacturers' sizing removal guidelines. To simulate the pyrolysis recycling process, the CFP fibres were heated in a furnace at 550 °C for 10 min [20]. The change in fibre mass during the processing time in nitrogen was approximately 1 % after 10 min, as shown by the thermogravimetric analysis (TGA) data presented in Fig. 1. The mass change is from a combination of the sizing removal (0.3 %) and change in moisture levels. The fibres were subsequently put in a water bath in an ultrasonic cleaner for 30 min, before being dried at 80 °C for a week. For the CFS fibres, 2 g of virgin T700 carbon fibres were soaked in 100 cm^3 of acetone for a week at room temperature. The fibres were then washed three times using fresh acetone and then refluxed in 200 cm^3 of boiling tetrahydrofuran (THF) for 72 h. The fibres were washed a further three times with fresh THF and then dried at 80 °C for a week.

Polypropylene microdroplet formation

The method used for producing carbon fibre/polypropylene microdroplet samples was the same as in [15]. Individual pellets of PP were initially melted on a hot plate at 190 °C. Tweezers were used to pull the molten polymer into a long fibre, to an uncontrolled diameter. The long PP fibres were then cut

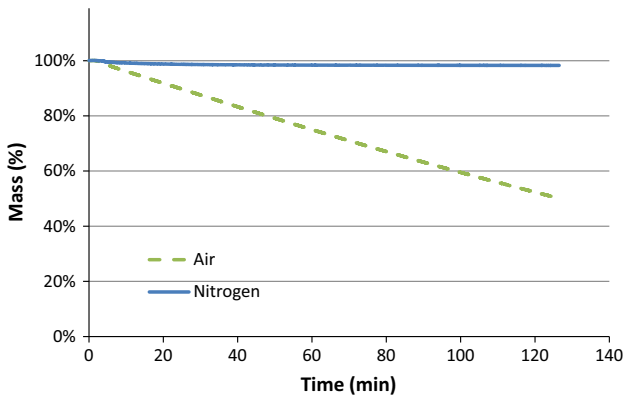

Figure 1 TGA data to show the mass change of T700 carbon fibre as a function of time. Fibres were heated to 550 °C in both nitrogen and air environments at a rate of 100 °C/min.

Table 1 Summary of properties for materials used in this study (manufacturer's data)

Property	density (g/cm^3)	UTS (MPa)	Modulus (GPa)
Carbon fibre (T700SC-60E)	1.78	4900	230
Polypropylene (Sabic 576P)	0.91	43	1.9
Epoxy (DLS1776)	1.18	55.3	3.15

into ~30 mm lengths to make it easier to attach them to the filaments. The residence time of each pellet on the hot plate was 30–60 s, significantly less than the time required to initiate matrix degradation (discussed in more detail in "The effect of fibre sizing" Section).

Single carbon fibres were suspended from a backlit panel to assist with viewing, using a small amount of tape at each end to maintain tension whilst preparing the samples. The polymer fibre was tied around the carbon filament using two pairs of tweezers. The volume of the polymer droplet was controlled, to an extent, by cutting the loose ends of the knot; regulating the fibre embedded length and the droplet diameter. Droplets were formed in a nitrogen-purged oven for the non-degraded samples and in the same oven under atmospheric conditions for the degraded samples. The oven temperature was set to 210 °C and the samples were maintained at this temperature for 6 min to ensure sufficient wetting.

Epoxy microdroplet formation

The epoxy was heated to 65 °C on a hot plate to melt the resin, enabling it to be pulled into a fibre, but critically for this system did not cure it. The epoxy was much more brittle than PP, preventing it from being tied onto the carbon fibre. A soldering iron was used to apply heat to an epoxy strand, making it coil around the fibre. These samples were transferred to a preheated oven at 125 °C to cure for 25 min, in accordance with the manufacturer's cure cycle.

All formed samples were transferred to individual card tabs to control the fibre free length (shown schematically in Fig. 2) and ensure alignment in the loading direction. A hole was punched in the card tab in-line with the loading axis to attach the sample to the tensile testing equipment.

Experimental methods

Single filament tensile test

Single fibre tensile testing (SFTT) was used to measure the tensile strength of the as-received carbon fibre and pseudo-recycled fibres to determine whether any damage had been introduced into the fibre during sizing removal. Tests were conducted in accordance with ISO 11566:1996 [21]. A single carbon filament was extracted at random from a fibre tow and glued to a paper frame using an epoxy resin (X60450, Force UK). 30–35 samples were manufactured for each fibre type to provide suitable confidence limits.

The fibre diameter was measured by a laser micrometer to enable calculation of the fibre tensile strength from the fibre cross-sectional area and recorded load. The gauge length of the fibre was kept constant at 20 mm. The characteristic strength is very sensitive to the gauge length and a number of authors have performed scaling analyses to allow extrapolation of data to lengths that are difficult to test [22, 23]. However, a 20 mm gauge length was equal to the effective fibre length used for the microbond test and enabled relatively easy preparation of samples compared to shorter lengths. The sample was gripped in a Hounsfield Series S testing machine, via a 5 N load cell (range: 0.1–5 N, resolution: 10^{-4} N), and tested at

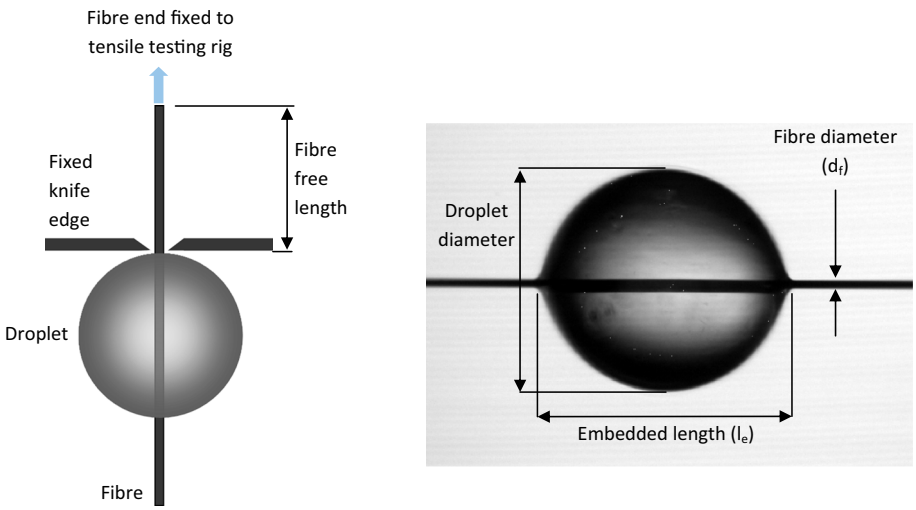

Figure 2 Schematic of microbond test set-up (*left*) and CF.Epoxy droplet viewed by optical microscopy (*right*).

room temperature with a cross-head speed of 1 mm/min until failure.

Weibull analysis was subsequently used to characterise the fibre strength, which is a widely used method for this procedure. The two-parameter model is commonly used for the analysis of brittle fibres [12, 15, 24], as the three-parameter analysis has been previously been shown to lead to unrealistic results [25]. The general three-parameter model was simplified to a two-parameter model by assuming that the threshold stress, σ_{th}, is equal to zero for brittle materials [24]

$$P_{(\sigma)} = 1 - \exp\left[-\delta V\left(\frac{\sigma - \sigma_{th}}{\sigma_0}\right)^m\right], \quad (1)$$

where $P_{(\sigma)} = 0$ for $\sigma < \sigma_{th}$.

$P(\sigma)$ is the probability of fibre failure, δV the change in volume, σ the applied stress, σ_{th} the threshold stress, σ_0 the Weibull scale parameter and m the Weibull shape parameter.

A probability estimator was used to calculate the probability of fibre failure ($P_{(\sigma)i}$) for the ith strength:

$$P_{(\sigma)i} = \frac{i - \alpha}{N - \beta}, \quad (2)$$

where N is the number of samples tested, which were sorted into ascending order and assigned a rank value (i), and α and β are statistical parameters that are commonly set to $\alpha = 0.5$ and $\beta = 0$ [25]. These values were used, since they give a less biased value of the shape parameter for a sample size of less than 50 specimens [24].

Equation 1 was subsequently rearranged to give Eq. 3, where the Weibull parameters σ_0 and m could be estimated using a linear least squares regression analysis. The characteristic strength (Weibull scale parameter) σ_0, is the maximum strength that 63 % of the weakest fibres in the population can achieve [26]. The shape parameter m describes the spread of the strength distribution, where lower values indicate a broader distribution.

$$\ln\left[-\ln\left(1 - P_{(\sigma)}\right)\right] = m.\ln(\sigma) - m.\ln(\sigma_0). \quad (3)$$

Microbond test

The microbond test has been widely used to establish the interfacial behaviour between different fibre/matrix combinations [12, 27–29]. A typical microbond force–displacement plot is shown in Fig. 3, indicating four key stages. The load–displacement curve is initially linear (Stage 1) as the microdroplet specimen deforms elastically. Debonding starts to occur at Stage 2, leading to stable crack propagation at the interface, with friction between the crack faces. Unstable crack growth occurs at Stage 3, leading to a large reduction in force and complete interfacial debonding. Dynamic frictional sliding occurs as the debonded droplet slides along the filament at Stage 4. The peak force at Stage 3 is used to calculate the apparent interfacial shear stress (IFSS). There is debate in the literature as to whether the assumptions for the calculation of IFSS in this way are valid for the systems tested [30]. The deformation associated with debonding is assumed to be elastic, although some authors have noted that plastic deformation can occur for thermoplastic systems [31], potentially invalidating results. The calculation for apparent IFSS also assumes that the stress along the interface is constant, which is a simplification, as the shear-lag approach [32, 33] and FEA modelling [34, 35] have both shown it varies along the embedded length. A constant interfacial stress also implies that failure is more sudden, with no account for the progressive "unzipping" due to interfacial crack propagation. It is possible for the interface to be in two different states when the applied force is at its maximum (F_{max}), with some regions still intact and some having debonded. In this situation, the apparent IFSS includes a large frictional contribution (from the debonded region), whose contribution increases with increasing embedded length. Therefore, apparent IFSS is only indirectly related to "interfacial adhesion" or "interfacial bonding", but it is still an effective way to distinguish between "weak" and "strong"

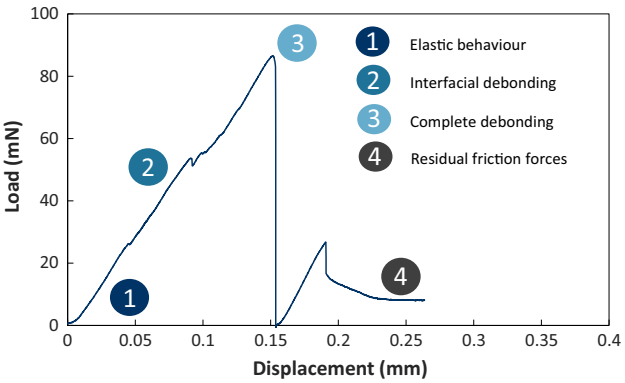

Figure 3 Microbond force–displacement plot for VCF.mPP.

interfacial interactions for assessing the efficiency of fibre sizings and coupling agents. The microbond test is therefore useful for determining apparent IFSS and is less labour intensive than other methods, enabling a large number of repeats to be carried out to reduce some of the uncertainty in the data analysis.

Approximately, 400 microbond samples were prepared and tested in the current work to obtain the experimental data. The fibre diameter, droplet diameter and the embedded length were measured for each specimen using optical microscopy. The variability for the diameter of the carbon filaments was much lower than in other systems such as glass fibre, which typically have distributions of around 10 μm [36]. The cumulative frequency distributions for the fibre diameters are presented in Fig. 4. The diameter distributions have been separated by fibre treatment, as removing the fibre sizing reduces the average diameter from 7 to 6.8 μm for both solvolysis and pyrolysis treatments.

The card tabs were suspended from the punched holes, using a steel hook attached to a 10 N load cell on an Instron tensile testing machine (Model 3342). A fixture [36] comprising two knife edges, which are movable by micrometer heads, constrained the droplet vertically. The knife edge separation could be finely controlled by the micrometers and was kept constant (10 μm spacing) for each test. The positioning of the knife edges was aided by the use of a stereo microscope at ×45 magnification. The test was carried out at a constant rate of 0.1 mm/min.

Samples that failed due to fibre failure were not included in the results. Approximately, 20 tests were used to obtain the average values for the apparent IFSS for each scenario. The apparent IFSS (τ_{app}) was calculated using the following equation:

$$\tau_{app} = \frac{F_{max}}{\pi d_f l_e}, \tag{4}$$

where F_{max} is the peak force recorded on the force/displacement curve, d_f the fibre diameter and l_e the embedded length. For the purposes of ease of testing, reduction of data and comparison with other values in the literature, the peak load is plotted against the embedded area and the linear fit is forced through the origin (according to Eq. 4). Samples were re-examined under a microscope after testing to check if adhesive failure had occurred and for re-measurements of the embedded length.

The theoretical maximum embedded length can be calculated by balancing the tensile failure stress of the fibre against the apparent shear stress at the interface. This can be used to determine the point at which the failure mode changes from interfacial failure to fibre failure and is calculated by rearranging Eq. 4:

$$L_e < \frac{\sigma_0 d_f}{4\tau_{app}}, \tag{5}$$

where L_e is the embedded length, σ_0 the characteristic fibre strength, d_f the fibre diameter and τ_{app} the apparent interfacial shear strength.

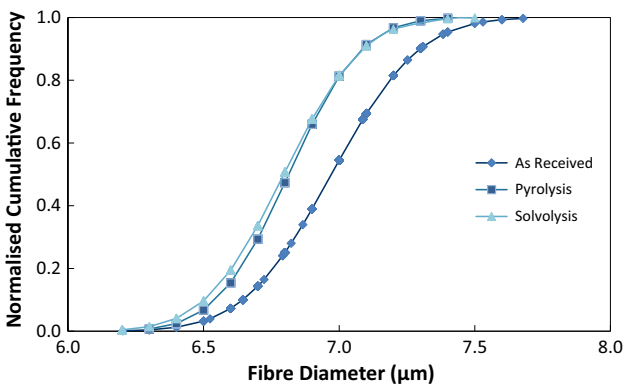

Figure 4 Cumulative distribution plot for fibre diameters obtained from the microbond test.

Matrix oxidation

The oxidation induction time was measured in accordance with BS 2782:Method 134A to confirm that the polypropylene was degrading during melting in air. A TA Instruments Q2000 DSC was used to heat the virgin polypropylene at 10 °C/min over the range of 190–240 °C.

Surface roughness measurements

Atomic force microscopy (AFM) was used to characterise the topology of the carbon fibres. A glass slide was used as the substrate for the carbon fibres. Two strips of Araldite were applied along the top surface of the slide at the extremities of the longest edges, which allowed a large section in the middle (with no adhesive) for the carbon fibres to be analysed. Single fibres were then extracted from the fibre bundles and laid perpendicular to the applied resin. The ends of the fibre were gently pulled to ensure that the fibre was straight and that it was in direct

contact with the glass slide. The adhesive was cured at room temperature for 6 h according to the manufacturer's data.

A Veeco Dimension 3000 SPM system atomic force microscope (AFM) was used to measure the surface roughness of the recovered fibres. The AFM was used in tapping mode and a scan area of 2 μm × 2 μm was measured for each sample. 12 scans were carried out for each fibre type, with 2 scans per fibre. An open-source analysis package (Gwyddion, Czech Metrology Institute) was used to analyse the output and calculate the R_a and R_z values. The background curvature of the fibre was removed by a second-order polynomial algorithm and the R_a and R_z values were calculated using a moving average calculation.

Surface composition

Surface chemical composition measurements were characterised by X-ray photoelectron spectroscopy (XPS). The samples for XPS were made by applying double-sided tape to a stainless steel mounting disc and subsequently covering the tape with the fibre tow to be analysed. The XPS analysis was performed using a Kratos Axis Ultra with a mono-chromated Al kα X-ray source (1486.6 eV) operated at 15 mA emission current and 10 kV anode potential. Survey spectra in the range of 0–1400 eV were recorded for each sample with a pass energy of 80 eV and a step of 0.5 eV, followed by high-resolution scanning over the C1 s range with a pass energy of 20 eV. All spectra were recorded at a 90° take-off angle. The surface atomic composition was calculated using Casa XPS software with Kratos sensitivity factors.

Curve fitting of the XPS high-resolution spectra was also carried out using the CasaXPS software, using a Gaussian–Lorentzian product function with a Shirley-type background. The G/L mix was taken as 0.5 for all peaks, except the main graphitic peak, which was taken as 0.8 with an exponential asymmetric blend tail [37].

Results and discussion

The effect of fibre sizing

A carbon fibre/epoxy (VCF.EP) benchmark was tested to assess how the experimental set-up for interfacial shear strength characterisation compared with other values in the literature. Samples were produced using the virgin fibre (with epoxy sizing) only. It was found that the VCF.EP benchmark had an apparent IFSS of 45.8 ± 4.6 MPa, which is within the range of values reported in the literature for similar systems [26, 38, 39]. A summary of the recorded IFSS data is given in Table 2.

Figure 5 shows the embedded area versus peak load plots for the polypropylene samples (VCF, CFP

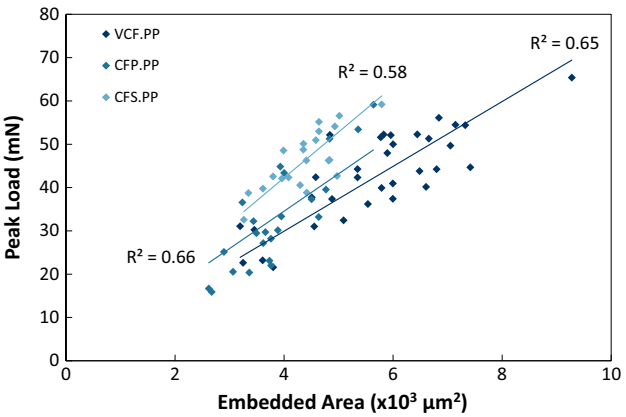

Figure 5 Peak force vs. embedded area for VCF, CFP and CFS with unmodified PP.

Table 2 Summary of interfacial shear strengths and confidence levels for tested droplets

Sample	IFSS (MPa)		Successful tests	Total tests	Confidence level (%)
	τ_{avg}	st dev			
VCF.PP(degraded)	3.4	1.2	31	32	97
VCF.PP (non-degraded)	8.0	2.2	35	37	95
CFP.PP	8.3	1.8	25	30	83
CFS.PP	10.6	1.0	21	25	84
VCF.mPP	31.6	4.8	26	86	30
CFP.mPP	35.9	2.6	16	51	31
CFS.mPP	36.2	2.9	22	47	47
VCF.epoxy (benchmark)	45.9	4.6	17	67	25

and CFS) with different fibre sizing treatments. Removing the epoxy sizing by pyrolysis and solvolysis both resulted in an increase in IFSS (gradient of line). The CFP.PP and CFS.PP samples exhibited an 8 and 38 % increase in IFSS, respectively, over the baseline VCF.PP (non-degraded). Mechanical interaction between the fibre and matrix accounted for most of the interface strength, as chemical bonds are not formed at the surface between unsized carbon fibre and unmodified polypropylene [6]. Atomic force microscopy (AFM) was used to characterise the topology of the fibre and assess whether the increase in IFSS for the unsized fibres can be attributed to changes in the surface roughness, where a rougher fibre would increase mechanical 'keying'. AFM results are presented as a root mean square roughness, R_{RMS}, and mean roughness, R_a, as summarised in Table 3. The CFS fibre had the lowest percentage increase between the R_a and R_{RMS} values, indicating that the surface was more homogeneous than the two other fibres. The virgin fibre had the highest percentage increase between R_a and R_{RMS}, which implies that the virgin fibre had more surface anomalies than the other fibres. Figure 6 shows that the high surface roughness for the virgin fibre was primarily due to irregular lumps on the surface. Inspection of phase lag plots obtained during AFM confirmed that these lumps were residual epoxy sizing that had fractured off adjacent fibres when the filament had been extracted from the bundle. There was no change in phase lag between these lumps and the epoxy surface coating on the fibre, suggesting that the lumps were the same material.

Table 3 Results from AFM microscopy on the surface roughness of the fibres. Scan area was 2 μm × 2 μm

	Fibre type		
	VCF	CFP	CFS
RMS roughness, R_{RMS} (nm)	15.5	5.9	4.0
Mean roughness, R_a (nm)	11.5	4.5	3.1
Max height (nm)	77.5	45.3	43.4

The phase lag plots for the CFP fibres showed a non-uniform surface (Fig. 7), which indicated that there was a very thin residual coating present on the surface of the fibre. Jiang et al. [19] noted that char formed on the surface due to decomposition of epoxy during a similar thermal recycling process. In contrast to the CFP fibres, the phase lag plot for the CFS fibres (Fig. 7) showed a uniform surface, which suggests that the sizing had been completely removed. The apparent IFSS for the CFS fibre system was the highest (10.6 ± 1.0 MPa). AFM inspection therefore indicated that changes in surface roughness were not responsible for increasing the mechanical interaction between fibre and matrix for the unsized fibres. However, removal of the sizing layer appeared to improve the adhesion between the fibre and matrix, which is attributed to the removal

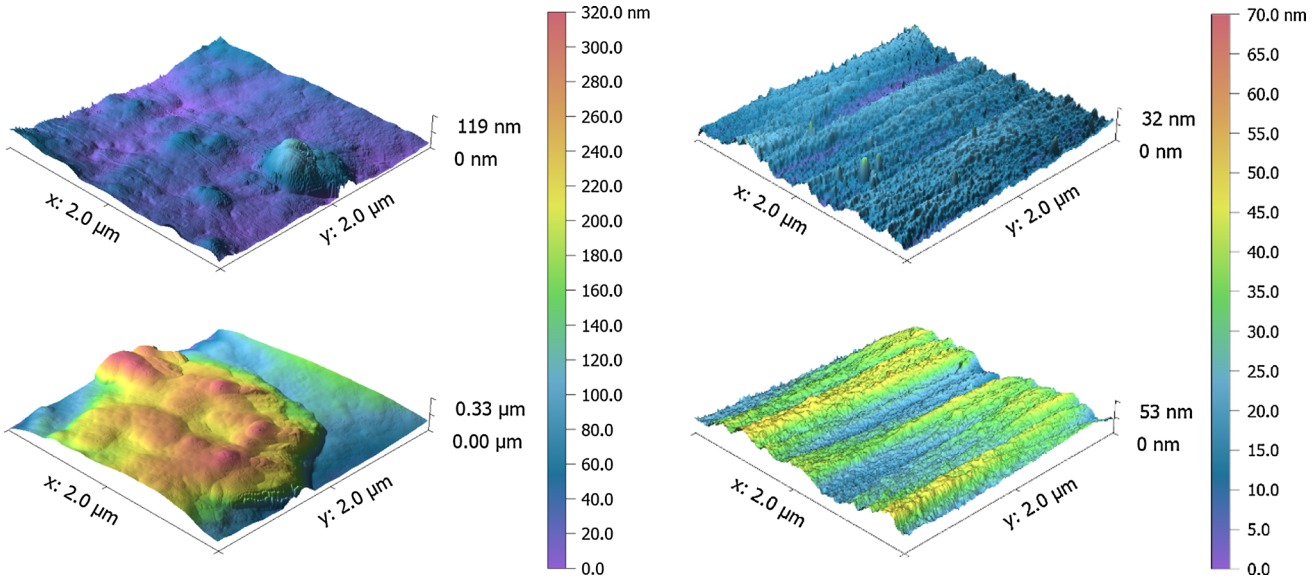

Figure 6 AFM images showing (*left*) examples of large features present on the VCF fibre and (*right*) smooth surface on CFS fibre.

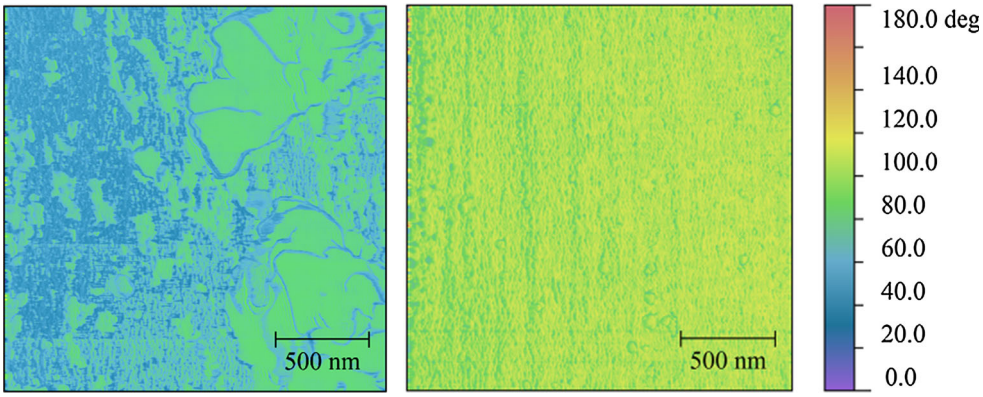

Figure 7 AFM phase lag plots for CFP (*left*) showing inhomogeneity on the surface and CFS (*right*) showing a uniform surface.

Table 4 Surface composition of VCF, CFP and CFS, including oxygen to carbon ratio (O/C) and nitrogen to carbon ratio (N/C)

Fibre Type	Photopeaks			Ratios	
	C 1 s	O 1 s	N 1 s	O/C	N/C
VCF At (%)	76.4	22.8	0.8	0.30	0.010
CFP At (%)	81.6	14.2	3.1	0.17	0.038
CFS At (%)	80.6	16.0	3.4	0.20	0.042

of a weaker tertiary interphase layer between the fibre and matrix.

XPS analysis of the three fibre types has been conducted to analyse the change in surface functionality due to sizing removal. The survey results for VCF, CFP and CFS are summarised in Table 4. The VCF fibre surface was primarily composed of carbon and oxygen with trace amounts of nitrogen, silicon and sodium, potentially left from the fibre manufacturing process [20]. The desized fibres (CFP and CFS) were also mainly composed of carbon and oxygen, but had higher proportions of nitrogen, sodium and silicon compared to the VCF fibre, which was consistent with observations reported in the literature for T700 fibres [20, 40]. The relative increase in nitrogen content for the CFP and CFS fibres was due to either incomplete carbonisation of the polyacrylonitrile precursor or surface treatments applied at the end of the fibre manufacturing process [41]. In either case, the increased presence of nitrogen confirmed that the sizing layer had been removed. The concentration of nitrogen has been reported to correlate with interfacial bonding strength, where nitrogen-containing groups such as CONH and NO_2 are known to be fundamental to adhesion performance in thermoplastic compatible sizings [42].

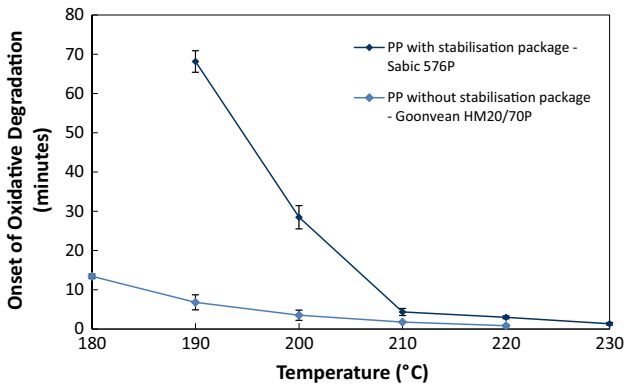

Figure 8 Oxidative induction time for polypropylene with and without stabilisation package to prevent degradation.

The effect of matrix degradation

A suspected cause for the low interfacial strength results published for CF.PP systems is polymer degradation, which can occur during droplet formation. The following section investigates the sensitivity of the apparent IFSS of CF.PP systems to environmental conditions during sample preparation, to ensure the data collected from the microbond test is representative of the interfacial behaviour in a composite component. Figure 8 shows the effect of oven temperature on the oxidation induction time (OIT) of the polypropylene used in this study (Sabic 576P) and an alternative polypropylene (Goonvean HM20/70P) without a stabilisation package (additives added by the manufacture to prevent, amongst other things, thermo-oxidative degradation). It is clear that the polypropylene with the stabilisation package is much less susceptible to thermal-oxidative degradation. However, at elevated temperatures commonly used to form microdroplets, circa 210 °C, even the PP with the stabilisation package starts to degrade after only

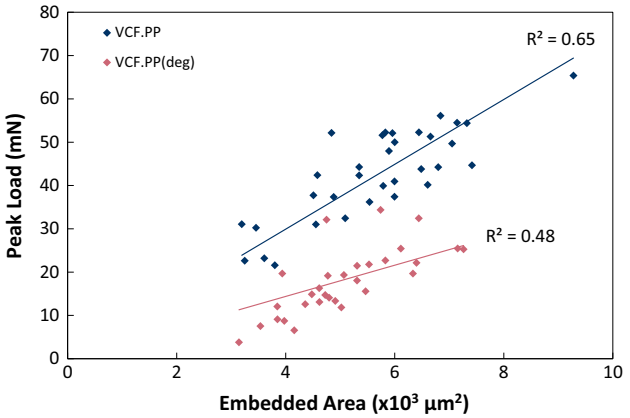

Figure 9 Peak force vs. embedded area for degraded and non-degraded samples.

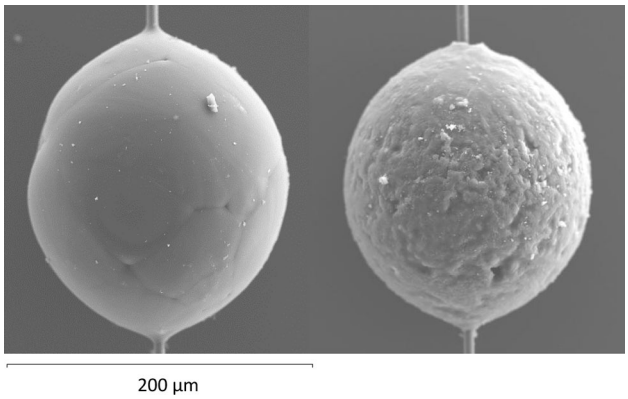

Figure 10 SEM images of non-degraded (*left*) and degraded (*right*) microbond samples after testing.

4 min of exposure. The large surface-to-volume ratio of PP microdroplets can further facilitate the process of thermo-oxidative degradation. The risk of degradation may also be increased as precise temperature control may not be possible when inserting specimens into a hot oven, because the temperature may increase to compensate for losses when the door is opened. An increase in temperature to 230 °C reduces the OIT to 1.35 min for the PP with the stabilisation package. It is also worth noting that the mass of the DSC samples is approximately 1000 times greater than the microdroplets; therefore, the onset time of thermo-oxidative degradation could be even lower during droplet formation.

Figure 9 shows a plot of the peak force versus embedded area for the degraded and non-degraded VCF.PP samples (both Sabic 576P). The degraded microbond samples had an apparent IFSS of 3.30 ± 1.32 MPa, similar to that found in [12], whereas the non-degraded samples actually had an IFSS of 7.72 ± 1.34 MPa. This shows the significance of good sample preparation and confirms that exposing the polypropylene to elevated temperatures, for even a very short period of time, can have a significant impact on the degradation of the polymer and therefore the interfacial properties. Similar findings were presented by Yang and Thomason [43] for glass fibre-reinforced polypropylene. The modulus of the PP and the coefficient of linear thermal expansion both reduce as the level of polymer degradation increases, reducing the compressive radial residual stress at the fibre/matrix interface during droplet formation. Figure 10 shows the difference in surface topology as observed by SEM of typical degraded and non-degraded polypropylene microbond samples after testing. The degraded sample had a rough and pitted surface, which is a common phenomenon referred to as 'chalking' in polymer degradation [44]. The non-degraded sample had a smooth surface with visible spherulite boundaries formed during crystallisation.

The coefficient of variation of the IFSS values is higher for the degraded system (35 %) than the non-degraded system (27 %), as larger droplets tend to have a higher than expected IFSS and smaller droplets have a lower than expected IFSS value. This result is consistent with the observations from earlier work [43] and is due to smaller droplets having a larger surface-to-volume ratio. A greater percentage of the polymer is exposed to oxygen per unit time, therefore causing a higher level of degradation in smaller droplets. This may therefore explain why linear regression of the data points from the degraded sample does not appear to fit through the origin particularly well.

The effect of fibre degradation

Single fibre tensile testing was used to measure the tensile strength of the VCF and pseudo-recycled fibres (CFS and CFP) to determine the effect of the recycling process on the ultimate tensile strength. Figure 11 shows the Weibull plots for data recorded from the tensile tests using a two-parameter unimodal Weibull analysis. The linear regression lines represent the strength distribution for each system and characteristic strengths were calculated at $\ln[-\ln(1/(1-\mathrm{Pf}))] = 0$. There is good agreement between all experimental data and the corresponding

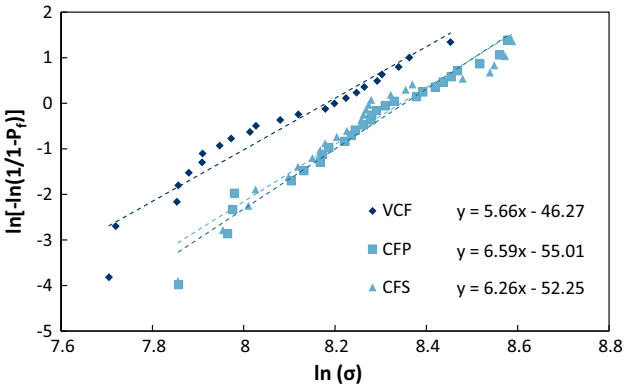

Figure 11 Weibull coordinate plot for single fibre tensile testing for the three fibre treatments used in this study.

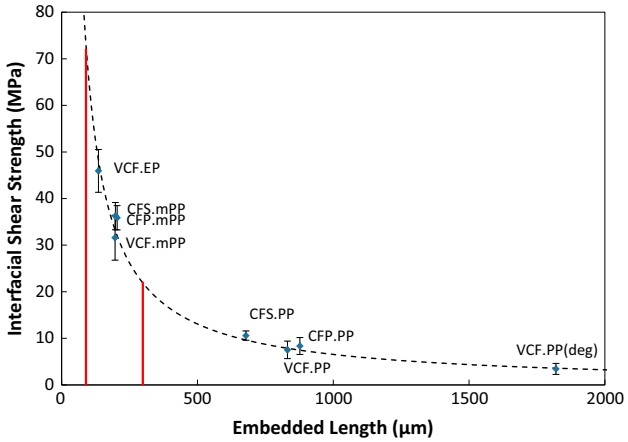

Figure 12 Maximum theoretical embedded length as a function of apparent IFSS values from microbond testing. Bounds indicate the range of practical polypropylene droplet sizes.

Weibull fits, with values close to others reported in the literature for carbon fibre at a gauge length of 20 mm [45, 46]. The Weibull parameters obtained are summarised in Table 5.

The average fibre strength of the CFP and CFS samples increases by 18–19 % following sizing removal, compared to the VCF samples. The Weibull modulus also increases by 16 and 11 %, respectively, for the CFP and CFS fibres over the VCF, indicating greater spread in the data for the non-sized samples. This is in line with observations in the literature, where increases in tensile strength have been observed for sizing removal in high modulus fibres (Toray M40) at the same 20 mm gauge length [47]. The Weibull moduli also agree well with other data in the literature [48–51], albeit they tend to be at the lower end of the range of values reported (4.5–10).

Results from this study confirm that the fibre strength was not adversely affected by removing the sizing. There was a marginal increase in the breaking loads recorded from the SFTT for the CFP and CFS fibres (7–8 %) over the VCF fibre, from 110 ± 27 mN to 118 ± 19 mN and 119 ± 25 mN, respectively, which was within the experimental scatter. The fibre diameter for the CFP and CFS fibres was on average 0.2 μm smaller (Fig. 4) than the as-received fibres, which is an order of magnitude larger than the thickness of sizing layers reported in the literature [52]. This implies that the outer layer of carbon fibre may have become detached during sizing removal or subsequent washing. Highly oriented graphitic planes are formed on the outer surface of carbon fibre by heat treatment during manufacture [53]. This highly aligned outer layer is typically 1.5 μm thick [53] and relatively weak [54, 55], and removal of this layer can increase the tensile strength [56] and improve the interface strength in carbon fibre/epoxy systems [57]. It has also been suggested that the removal of the outer layer removes surface flaws, which are known to be a significant factor for tensile strength properties [56].

The maximum theoretical embedded lengths have been calculated using the fibre strengths of the three fibre types that have been tested (see Table 5). Figure 12 shows the relationship between embedded length and interfacial shear strength for the fibre strengths recorded from the single fibre tensile test. The range of available embedded lengths decreases as the interface strength of the fibre/matrix system increases, which reduces the reliability of the

Table 5 Carbon filament strength data obtained from single fibre tensile testing and Weibull parameters

Fibre	Fibre tensile strength (GPa)		Shape parameter	Characteristic strength (GPa)	Samples
	Avg	St dev			
VCF	3.3	0.69	5.66	3.57	23
CFP	3.96	0.72	6.59	4.24	27
CFS	3.91	0.76	6.26	4.21	25

apparent IFSS value obtained from linear regression. The range of suitable embedded lengths for carbon fibres is shown in Fig. 12 by red vertical lines, ranging from 90 to 300 μm. Droplets with embedded lengths of less than 90 μm were extremely hard to prepare due to the small amount of polymer needed, and droplets with embedded lengths of over 300 μm were often non-axisymmetric. The theoretical maximum embedded length was approximately 200 μm for interface strengths of 35 MPa; therefore, the range of available embedded lengths was effectively halved, explaining the reduction in yield at higher IFSS values (see confidence levels presented in Table 2).

The effect of coupling agent

The apparent IFSS values recorded for the VCF reinforced PP range from 3.4 to 10.6 MPa, which are significantly lower than the VCF Epoxy system at 45.9 MPa. The addition of maleic anhydride is shown to improve the IFSS for all carbon fibre/polypropylene systems under investigation. Figure 13 shows a plot of the peak force as a function of embedded area for the VCF.PP and VCF.mPP. Introducing mPP at 2 %wt increased the apparent IFSS of the VCF.PP (non-degraded) system by 320 %, from 7.72 ± 1.34 to 32.64 ± 4.05 MPa. Figure 14 shows the influence of increasing the maleic anhydride content on the properties of the baseline PP. It is clear that there is no change in the ultimate tensile strength, the tensile stiffness and the yield strain for MPP additions of up to 12 %wt. This was unexpected, as the mechanical properties are typically linked to the molecular weight [58], but this effect has previously been reported for modified polypropylene [59, 60]. The increase in IFSS from adding 2 %wt maleic anhydride can therefore be attributed to improved interfacial bonding between the carbon fibre and PP, rather than an increase in bulk properties. The reactive grafted polypropylene diffuses to the fibre surface and forms both covalent and hydrogen bonds with hydroxyl groups. For the VCF.PP, the IFSS is governed by weak physical forces which are influenced by the fibre topology and residual stresses formed during cooling.

Figure 15 shows a selection of SEM micrographs taken from VCF.EP (benchmark), VCF.PP and VCF.mPP microdroplet specimens. The increase in interface strength due to the addition of the maleic anhydride coupling agent resulted in a change in failure mode at the contact point with the knife edges. Failure of the VCF.mPP specimens was similar to the VCF.EP specimens, with a small part of the meniscus left behind on the fibre after debonding. Completely clean fibres were observed for the lower interface strength systems. Figure 16 shows higher magnification images of the meniscus left behind on the fibres for the VCF.EP and VCF.mPP samples. There was no discernible difference in the shape of the residual meniscus between the two samples, with both exhibiting brittle failure characteristics. The force/displacement curves for samples exhibiting meniscus failure (see Fig. 17) were significantly different compared to those where the droplet completely debonded. Samples with lower interfacial strength (VCF.PP) experienced a significant reduction in force

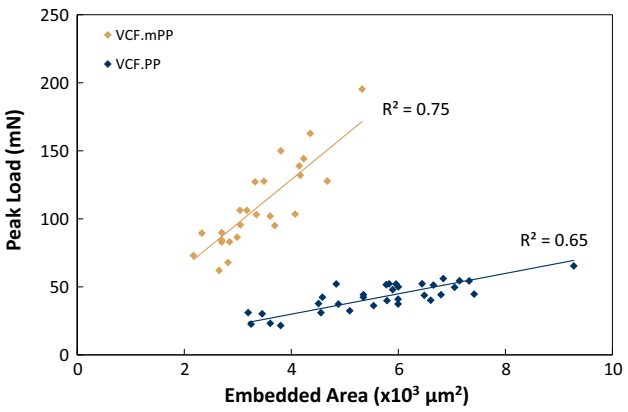

Figure 13 Peak force vs. embedded area for CF.PP with and without maleic anhydride.

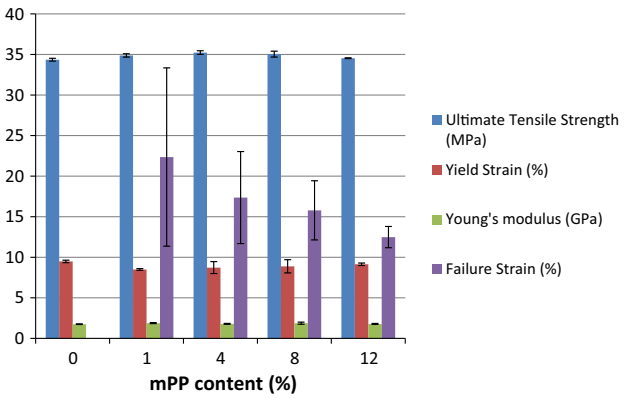

Figure 14 Influence of increasing additions of maleic anhydride on the tensile properties of PP. Failure strain of virgin polymer was not recorded, as it exceeded 40 %.

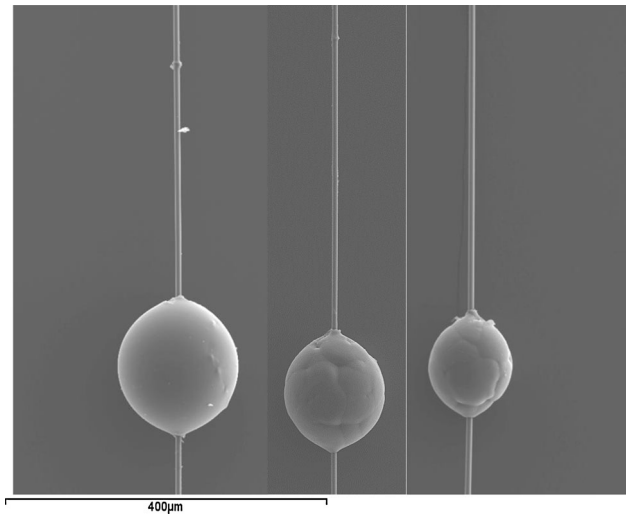

Figure 15 SEM micrographs of (*left*) a debonded CF.EP microdroplet with detached meniscus (*middle*) CF.mPP microdroplet also with detached meniscus and (*right*) CF.PP microdroplet without a detached meniscus.

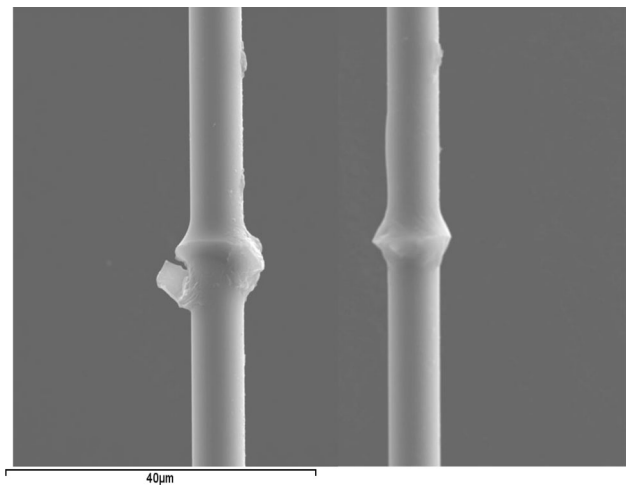

Figure 16 SEM micrographs of the meniscus from (*left*) a VCF.EP microdroplet and (*right*) a VCF.mPP microdroplet, both after debonding.

following complete debonding. A constant residual force was then recorded due to frictional sliding. The force/displacement curves for samples that experienced meniscus failure (higher interfacial strength systems, including VCF.EP and VCF.mPP) exhibited a characteristic sawtooth shape. The force suddenly reduces to zero at debonding and then partially recovers before another drop in load is observed due to a change in friction from static to dynamic. The force eventually reaches a plateau value which is

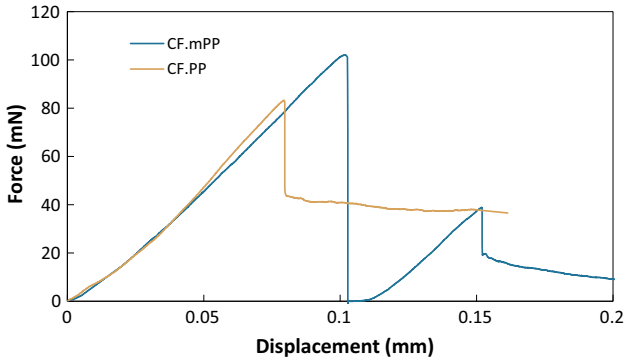

Figure 17 Characteristic force displacement traces for high interface strength tests (e.g., VCF.mPP) and low interface strength tests (e.g., VCF.PP).

proportional to the dynamic friction. Complete load loss at debonding is likely caused by the release of strain in the fibre, coupled with the fibre undergoing Poisson's shrinkage at high fibre strain values [54]. This would result in the fibre contracting whilst the droplet was sliding at low friction, causing the droplet to 'jump' a section of the fibre [15]. Gaps of up to 60 µm have been recorded during testing between final debonding and resumed contact of the knife edges on the droplet, although no correlation has been found between the length of gap and embedded length, droplet size or force.

The modified PP was also combined with the CFP and CFS fibres to assess the compatibility of the maleic anhydride with the desized fibres. The interface strength increased by 330 % for the CFP fibres and 240 % for the CFS fibres, to 35.9 ± 2.6 and 36.2 ± 2.9 MPa, respectively. Statistically, there was no discernible difference between the CFS.mPP and CFP.mPP systems, given the level of experimental variation. There was, however, a measurable difference between these samples and the VCF.PP. The combination of adding a coupling agent and removing the epoxy sizing yielded the highest IFSS, where the effects of adding the coupling agent were more significant than removing the sizing agent. The addition of the coupling agent brought the IFSS values for the carbon fibre/polypropylene system in line with values reported in the literature for VCF epoxy [26, 38, 39]. The XPS analysis of the surface composition indicated an increase in nitrogen at the surface of the desized fibres. Nitrogen is known to facilitate ring opening and forming of amic acid with carbonyl anhydrides present in maleic anhydride [61]. Increases in interface strength seen for the desized fibres

can therefore be attributed to further chemical bonding as a result of reactions between the coupling agent and nitrogen functionalities.

The improvement in IFSS from adding the mPP coupling agent is much higher than values reported in the literature for a similar system. The apparent IFSS increased from 2.36 to 7.00 MPa with the addition of 8 %wt G3015 maleic anhydride in [12]. Whilst the carbon fibre (T600SC-60E) and polypropylene (100-GA12) grades used were different from the current study, the values reported in [12] were approximately 80 % lower than the values reported here, using the same microbond test. This can be attributed to mechanical degradation of the polypropylene, caused by oxidation [43], as discussed above. Samples for the current study were all prepared under nitrogen to avoid oxidative degradation and, consequently, the apparent IFSS approaches the shear strength of the matrix (approximately 40 MPa), which is the practical upper limit. Ash et al. [35] have shown that the interface strength could exceed the matrix shear strength, however, as a strengthening mechanism takes place while the matrix is under compressive normal stress. This was only predicted for brittle materials using Coulomb–Mohr theory; however, it is unclear how the ductile response of thermoplastic matrices would behave under the same conditions.

It is also important to note that the percentage of successful tests decreased with the addition of the mPP coupling agent (see Table 2). Figure 18 indicates that the failure mode of the microdroplet system changes as the interfacial strength increases, implying that the values recorded during this study may represent a lower bound. The force required to cause debonding increases as the embedded area increases (according to Eq. 4), which can exceed the failure load of the fibre if the interfacial shear strength of the system is high. The data agree well with the theoretical maximum embedded length (calculated using the experimental fibre data from Sect. 3.3), which implies that the embedded length should be less than ~200 μm for the VCF.mPP system. It is difficult to control the droplet formation, however, and the embedded length of each specimen can vary.

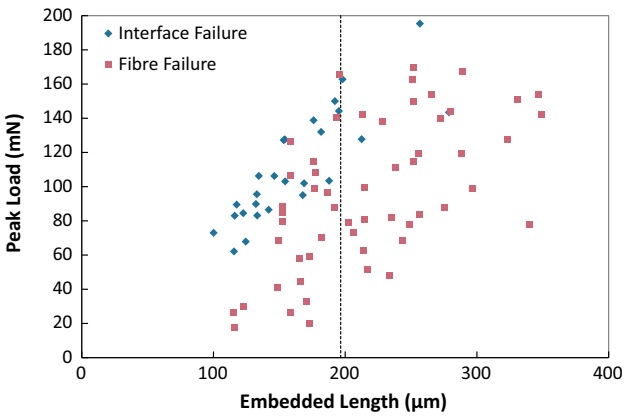

Figure 18 Summary of failure mode for VCF.mPP microbond samples. *Dotted vertical line* indicates theoretical embedded length limit.

Higher fibre failure loads may also partly explain why the CFP.mPP and CFS.mPP microbond samples showed improvements in IFSS over VCF.mPP. As the peak fibre load was found to be higher for the two desized fibres, higher interface strengths could be tested, which may suggest that the average IFSS for the VCF.mPP was a lower bound result, as stronger interfaces could not be tested due to fibre breakage. The agreement between the increases in characteristic strengths compared with the increases seen in IFSS, between the three fibres, respectively, support this hypothesis. Additionally, the reduction in data scatter from the VCF to the desized fibres may also be explained by an increased range of embedded lengths available due to the increase in fibre strength.

Conclusions

The objective of this study was to investigate the feasibility of combining discontinuous recycled carbon fibres with polypropylene, to produce a low-cost, high specific stiffness material for high-volume applications. The quality of the fibre/matrix interface is known to dominate the mechanical performance and failure characteristics of discontinuous fibre composites. The inherent low affinity of carbon fibre and polypropylene was a major concern and has motivated a detailed study of the interfacial behaviour between the two materials.

The apparent interfacial shear strengths for a range of recycled carbon fibre/polypropylene systems have been measured using the microdroplet test, which have been compared against a carbon fibre/epoxy benchmark. Fibre recycling was simulated by two different methods; a furnace was used to burn the sizing to simulate a pyrolysis process and acetone

was used to wash off the sizing to simulate a solvolysis process. The removal of fibre sizing by pyrolysis yielded a 4 % increase in the IFSS over virgin fibre, and sizing removal by solvolysis increased the IFSS by 33 %. The addition of maleic anhydride had the largest effect on the IFSS, with a 320 % increase over the base polymer for the virgin fibres and 330 and 240 % increase for the CFP and CFS fibres, respectively. The combination of removing sizing by solvolysis and the addition of the coupling agent yielded an apparent IFSS value of 36.2 MPa, which approaches the shear strength of the polymer: the theoretical maximum IFSS value that can be achieved. This is pertinent, as it suggests that the polypropylene is able to adhere well to the fibre regardless of fibre sizing; however, further increases may be achieved when a thermoplastic compatible sizing is used.

The value of the IFSS for the maleic anhydride-modified samples was much higher than other values reported for similar systems in the literature, which suggests that other authors may have tested samples that have degraded during droplet formation. Matrix degradation is therefore a key factor in the interface strength measurement. The IFSS was 43 % higher for samples prepared under nitrogen, compared with those prepared under atmospheric conditions. The oxidation induction time was measured for polypropylene and revealed that degradation occurred after less than 3 min at typical sample-processing temperatures.

Acknowledgements

This work was conducted as part of the TARF-LCV project, funded by the UK Engineering and Physical Sciences Research Council, EPSRC (reference EP/I038616/1).

References

[1] Henning F, Ernst H, Brüssel R (2005) LFTs for automotive applications. Reinf Plast 49(2):24–33

[2] Krause W et al (2003) LFT-D—a process technology for large scale production of fiber reinforced thermoplastic components. J Thermoplast Compos Mater 16(4):289–302

[3] Biron M, Chapter 7—future prospects for thermoplastics and thermoplastic composites, in thermoplastics and thermoplastic composites. 2007, Elsevier: Oxford. pp. 829–861

[4] Pimenta S, Pinho ST (2011) Recycling carbon fibre reinforced polymers for structural applications: technology review and market outlook. Waste Manag 31(2):378–392

[5] Vaidya UK, Chawla KK (2008) Processing of fibre reinforced thermoplastic composites. Int Mater Rev 53(4):185–218

[6] Mukhopadhyay S, Deopura BL, Alagiruswamy R (2003) Interface behavior in polypropylene composites. J Thermoplast Compos Mater 16(6):479–495

[7] Tang L-G, Kardos JL (1997) A review of methods for improving the interfacial adhesion between carbon fiber and polymer matrix. Polym Compos 18(1):100–113

[8] Dai Z et al (2011) Effect of sizing on carbon fiber surface properties and fibers/epoxy interfacial adhesion. Appl Surf Sci 257(15):6980–6985

[9] Maligno AR, Warrior NA, Long AC (2010) Effects of interphase material properties in unidirectional fibre reinforced composites. Compos Sci Technol 70(1):36–44

[10] Greco A et al (2013) Thermal and chemical treatments of recycled carbon fibers for improved adhesion to polymeric matrix. J Compos Mater 47(3):369–377

[11] Karsli NG, Aytac A (2011) Effects of maleated polypropylene on the morphology, thermal and mechanical properties of short carbon fiber reinforced polypropylene composites. Mater Des 32(7):4069–4073

[12] Wong KH et al (2012) Effect of coupling agents on reinforcing potential of recycled carbon fibre for polypropylene composite. Compos Sci Technol 72(7):835–844

[13] Li M et al (2014) Synergetic effect of epoxy resin and maleic anhydride grafted polypropylene on improving mechanical properties of polypropylene/short carbon fiber composites. Compos A Appl Sci Manuf 67:212–220

[14] Han SH, Oh HJ, Kim SS (2014) Evaluation of fiber surface treatment on the interfacial behavior of carbon fiber-reinforced polypropylene composites. Compos B Eng 60:98–105

[15] Yang L, Thomason JL (2012) Development and application of micromechanical techniques for characterising interfacial shear strength in fibre-thermoplastic composites. Polym Testing 31(7):895–903

[16] Jannerfeldt G et al Matrix modification for improved reinforcement effectiveness in polypropylene/glass fibre composites. Appl Compos Mater 8(5):327–341
[17] Liakus J et al (2003) Processing-microstructure-property predictions for short fiber reinforced composite structures based on spray deposition process. Compos Struct 61(4):363–374
[18] Luchoo R et al (2010) Net shape spray deposition for compression moulding of discontinuous fibre composites for high performance applications. Plast Rubber Compos 39(3–5):216–231
[19] Jiang G et al (2005) Study of a fluidised bed process for recycling carbon fibre from polymer composites, in 7th World Congress for Chemical Engineering 2005: Glasgow, UK
[20] Jiang G et al (2008) Surface characterisation of carbon fibre recycled using fluidised bed. Appl Surf Sci 254(9):2588–2593
[21] Standard I (1996) Carbon fibre– determination of the tensile properties of single filament specimens, in BS ISO 11566. 1996
[22] Padgett WJ, Durham SD, Mason AM (1995) Weibull analysis of the strength of carbon fibers using linear and power law models for the length effect. J Compos Mater 29(14):1873–1884
[23] Asloun M et al (1989) On the estimation of the tensile strength of carbon fibres at short lengths. J Mater Sci 24(10):3504–3510. doi: 10.1007/BF02385732
[24] Davies IJ (2001) Empirical correction factor for the best estimate of Weibull modulus obtained using linear least squares analysis. J Mater Sci Lett 20(11):997–999
[25] Thomason JL (2013) On the application of Weibull analysis to experimentally determined single fibre strength distributions. Compos Sci Technol 77:74–80
[26] Jiang G et al (2009) Characterisation of carbon fibres recycled from carbon fibre/epoxy resin composites using supercritical n-propanol. Compos Sci Technol 69(2):192–198
[27] Thomason J (2010) Interfacial strength in fibre reinforced thermoplastics. in International Conference on Interfaces & Interphases in Multicomponent Materials (IIMM)
[28] Liu B et al (2013) Interfacial shear strength of carbon fiber reinforced polyphenylene sulfide measured by the microbond test. Polym Testing 32(4):724–730
[29] Huang YD et al (2002) Influence of ultrasonic treatment on the characteristics of epoxy resin and the interfacial property of its carbon fiber composites. Compos Sci Technol 62(16):2153–2159
[30] Zhandarov S, Mäder E (2005) Characterization of fiber/matrix interface strength: applicability of different tests, approaches and parameters. Compos Sci Technol 65(1):149–160
[31] Zinck P et al (2001) Are microcomposites realistic models of the fibre/matrix interface? I. Micromechanical modelling. Polymer 42(12):5401–5413
[32] Cox HL (1952) The elasticity and strength of paper and other fibrous materials. Br J Appl Phys 3(3):72–79
[33] Chen Z, Yan W (2015) A shear-lag model with a cohesive fibre–matrix interface for analysis of fibre pull-out. Mech Mater 91(1):119–135
[34] Pandey G, Kareliya CH, Singh RP (2012) A study of the effect of experimental test parameters on data scatter in microbond testing. J Compos Mater 46(3):275–284
[35] Ash JT et al (2013) Estimation of the true interfacial shear strength for composite materials with the microbond test, in ASME 2013 International Mechanical Engineering Congress and Exposition. San Diego, CA
[36] Yang L, Thomason JL (2010) Interface strength in glass fibre–polypropylene measured using the fibre pull-out and microbond methods. Compos A Appl Sci Manuf 41(9):1077–1083
[37] Viswanathan H, Rooke MA, Sherwood PMA (1997) X-ray photoelectron spectroscopic studies of carbon-fiber surfaces. 21. Comparison of carbon fibers electrochemically oxidized in acid using achromatic and monochromatic XPS. Surf Interface Anal 25(6):409–417
[38] Biro DA, McLean P, Deslandes Y (1991) Application of the microbond technique: characterization of carbon fiber-epoxy interfaces. Polym Eng Sci 31(17):1250–1256
[39] He J et al (2006) Controlled interface between carbon fiber and epoxy by molecular self-assembly method. Mater Chem Phys 99(2–3):388–393
[40] Liu WB et al (2013) Properties of carbon fiber sized with poly(phthalazinone ether ketone) resin. J Appl Polym Sci 128(6):3702–3709
[41] Cazeneuve C, Castle JE, Watts JF (1990) The structure of the interface in carbon fibre composites by scanning Auger microscopy. J Mater Sci 25(4):1902–1908. doi: 10.1007/BF01045740
[42] Grozdanov A, Bogoeva-Gaceva G (2010) Carbon fibers/polyamide 6 composites based on hybrid yarns. J Thermoplast Compos Mater 23(1):99–110
[43] Yang L, Thomason JL, Zhu W (2011) The influence of thermo-oxidative degradation on the measured interface strength of glass fibre-polypropylene. Compos A Appl Sci Manuf 42(10):1293–1300
[44] Singh B, Sharma N (2008) Mechanistic implications of plastic degradation. Polym Degrad Stab 93(3):561–584
[45] Meng L et al (2012) Comparison studies of surface cleaning methods for PAN-based carbon fibers with acetone, supercritical acetone and subcritical alkali aqueous solutions. Appl Surf Sci 261:415–421

[46] Yip HLH, Pickering SJ, Rudd CD (2002) Characterisation of carbon fibres recycled from scrap composites using fluidised bed process. Plast, Rubber Compos 31(6):278–282
[47] Marston C et al (1996) Failure characteristics in carbon/epoxy composite tows. Compos A Appl Sci Manuf 27(12):1183–1194
[48] Naito K et al (2011) The effect of gauge length on tensile strength and Weibull modulus of polyacrylonitrile (PAN)-and pitch-based carbon fibers. J Mater Sci 47(2):632–642
[49] Pickering KL, Murray TL (1999) Weak link scaling analysis of high-strength carbon fibre. Compos A Appl Sci Manuf 30(8):1017–1021
[50] Zhang RL et al (2011) Effect of emulsifier content of sizing agent on the surface of carbon fibres and interface of its composites. Appl Surf Sci 257(8):3519–3523
[51] Kettle AP et al (1997) Plasma polymerisation for molecular engineering of carbon-fibre surfaces for optimised composites. Compos Sci Technol 57(8):1023–1032
[52] Yuan H et al (2013) Improved interfacial adhesion in carbon fibre/polyether sulfone composites through an organic solvent-free polyamic acid sizing. Appl Surf Sci 279:279–284
[53] Lee SM (1992) Handbook of composite reinforcements, Wiley
[54] Piggott MR (1997) Why interface testing by single-fibre methods can be misleading. Compos Sci Technol 57(8):965–974
[55] Zhang H, Zhang Z, Breidt C (2004) Comparison of short carbon fibre surface treatments on epoxy composites: I. Enhancement of the mechanical properties. Compos Sci Technol 64(13–14):2021–2029
[56] Langston TA, Granata RD (2014) Influence of nitric acid treatment time on the mechanical and surface properties of high-strength carbon fibers. J Compos Mater 48(3):259–276
[57] Baillie CA et al (1993) Special issue microphenomena in advanced composites the influence of chemistry on the adhesion at the interface of carbon/epoxy composites. Compos Sci Technol. 48(1):97–102
[58] Qiu W, Endo T, Hirotsu T (2006) Structure and properties of composites of highly crystalline cellulose with polypropylene: effects of polypropylene molecular weight. Eur Polymer J 42(5):1059–1068
[59] Roux C, Denault J, Champagne MF (2000) Parameters regulating interfacial and mechanical properties of short glass fiber reinforced polypropylene. J Appl Polym Sci 78(12):2047–2060
[60] Rijsdijk HA, Contant M, Peijs AAJM (1993) Special issue microphenomena in advanced composites continuous-glass-fibre-reinforced polypropylene composites: i. influence of maleic-anhydride-modified polypropylene on mechanical properties. Compos Sci Technol 48(1):161–172
[61] Duin M, Borggreve RJM, Al-Malaika S (eds) (1997) Blends of polyamides and maleic-anhydride-containing polymers: interfacial chemistry and properties, in Reactive Modifiers for Polymers. Springer, Dordrecht, pp 133–162